A polarized nucleus-cytoskeleton-ECM connection in migrating cardioblasts controls heart tube formation

Dondi C, Bertin B, Da Ponte JP, Wojtowicz I, Jagla K and Junion G*

Université Clermont Auvergne, CNRS 6293, Inserm 1103, GReD institute, F-63000 Clermont-Ferrand, France

* Corresponding author
guillaume.junion@uca.fr
GReD Institute, 28 Place Henri Dunant, 63000 Clermont-Ferrand-FRANCE

Summary

CAP and MSP300 are involved in connecting the nucleus and extracellular matrix during heart formation, which leads to the maintenance of post-mitotic state of Tinman cardioblasts.

Key words

Cardioblast, Post-mitotic state, Cell alignment, *Drosophila*, Embryogenesis

Abstract

The formation of the cardiac tube is a remarkable example of complex morphogenetic processes conserved from invertebrates to humans. It involves coordinated collective migration of contralateral rows of cardiac cells. The molecular processes underlying the specification of cardioblasts (CBs) prior to migration are well established and significant advances have been made in understanding the process of lumen formation. However, the mechanisms of collective cardiac cells migration remain elusive. Here we identified *CAP* and *MSP300* as novel actors involved during CBs migration. They both exhibit highly similar temporal and spatial expression patterns in migrating cardiac cells and are necessary for the correct number and alignment of CBs, a prerequisite for the coordination of their collective migration. Our data suggest that CAP and MSP300 are part of a protein complex linking focal adhesion sites to nuclei via the actin cytoskeleton that maintains post-mitotic state and correct alignment of CBs.

Introduction

The genetic network regulating heart development is highly conserved from flies to humans with orthologous transcription factor (TF) families and signaling pathways essential for heart development such as Tinman/Nkx2.5, Pannier/GATA4-6, Tailup/Isl1, Dorsocross H15 Mid/Tbx, Hand, Dpp/BMP or Wg/Wnt (Bryantsev and Cripps, 2009; Busser et al., 2015; Jin et al., 2013; Junion et al., 2012; Lovato and Cripps, 2016). However, while mechanistic insights have been gained on the specification of cardiac progenitors, less is known about genes controlling subsequent events of cardiogenesis.

Just as in mammals, formation of the *Drosophila* heart starts by the migration of bilateral strips of cardiac progenitor cells to the midline and the assembly of a linear heart tube. Cardioblasts (CBs) migration occurs concurrently with dorsal closure, a process leading to the spreading of the epidermis dorsally over an extraembryonic epithelium, the amnioserosa. Migrating CBs extend projections from their dorsal surface and towards the leading edge of the epidermis suggesting coupling of these two tissues (Haack et al., 2014; Rugendorff et al., 1994). However, during the late phase of migration, CBs move cell autonomously. They send filopodia that contact contralateral CBs and ensure correct cell matching and linear heart tube assembly (Haack et al., 2014; Medioni et al., 2008, Zhang et al., 2018).

Some factors in this process have been identified including the transmembrane protein Toll (Wang et al., 2005) and faint sausage, which participates in adhesion between ipsilateral CBs (Haag et al., 1999).

Proteins involved in setting or maintaining polarity of CBs have also been implicated in collective migration. Among them the Integrin dimer expressed by the CBs (αPS3, βPS), its ligand Laminin-A and cytoplasmic Integrin adapter Talin are all required for proper CBs alignment (Stark et al., 1997; Vanderploeg and Jacobs, 2015; Vanderploeg et al., 2012).

Moreover, the coordinated migration and alignment of CBs requires the Slit morphogen and its receptor Robo (MacMullin and Jacobs, 2006; Qian et al., 2005). Slit function in cardiac cell migration is conserved from *Drosophila* to vertebrates. In zebrafish, Slit2 knock down embryos show disruption of endocardial collective cell migration with individual cells migrating faster and with loss of directionality (Fish et al., 2011).

Recent findings have shown a genetic interaction between αPS3 gene *scb* and *Slit/Robo*, suggesting an integrated function of cell membrane-associated factors in CB migration polarization during cardiac tube formation (Vanderploeg et al., 2012). The link between cell adhesion and actin cytoskeleton remodeling is also fundamental for CBs migration and

requires intermediate proteins to mediate connections and to transduce signals. Among them, two members of the Dock Guanine nucleotide Exchange Factors (GEFs) containing SH3 domain, Myoblast city and Sponge, are required during CBs migration through activation of Rac and Rap1, respectively (Biersmith et al., 2015). Mutants for these two genes revealed defects in the migrating CB rows with gaps and clusters of multilayered CBs. Moreover, the Rho GTPase CDC42 is required in Tinman CBs for the contact with the opposite row (Swope et al., 2014; Vogler et al., 2014) by modulating localization of non-muscle myosin II Zipper (Vogler et al., 2014). Thus, cytoskeleton modulations allow filopodia formation at the CBs leading edge and ensure coordinated, tension-mediated modification of cell shape to keep migrating CBs aligned.

Here we identify the SORBS Cbl Associated Protein (CAP) and Muscle Specific Protein 300 (MSP300) as novel mediators of the transition from mitotic state to CBs migration. *In vitro*, SORBS proteins are generally targeted to focal adhesion sites where they play diverse roles in mechano-transduction, contributing to stiffness sensing and contractility (Ichikawa et al., 2017). CAP is the only SORBS family member in *Drosophila* and has been described as an adaptor protein making links between different partners at the membrane-cytoskeletal interface of stretch-sensitive structures *via* the vinculin-integrin complex (Bharadwaj et al., 2013).

MSP300 is a large protein of the Nesprin family with several protein domains including spectrin and nuclear anchoring KASH domains. Nesprin provides a link between actin cytoskeleton and perinuclear layer via Linker of Nucleoskeleton and Cytoskeleton (LINC) (Mellad et al., 2011)

Recently, MSP300 has been shown to display stretching capacity participating in the elasticity of a myonuclear scaffold to protect myonuclei from mechanical stress (Wang et al., 2015).

Nucleus deformability is necessary when cells are squeezing through small constrictions during their migration (Friedl et al., 2011). The role of the nucleus in cell migration is suggested to be dependent on its connections with components of the cytoskeleton mediated by LINC and indirectly with extracellular matrix including focal adhesion complex (Fruleux and Hawkins, 2016).

In the developing heart, our data show that CAP and MSP300 accumulate in a punctate manner on apical and basal sides of migrating CBs. We also demonstrate that polarized accumulation of nuclei-anchored MSP300 and cell membrane associated CAP promote post-mitotic state and are required for CBs alignment, coordinated migration and proper CBs

nuclei shapes. These findings imply the requirement of polarized nucleus-cytoskeleton-ECM connections during collective CBs migration.

Results

CAP and MSP300 accumulate interdependently in apical and basal dots in migrating cardioblasts

Because coordinated CBs migration towards the midline involves stretch induced morphological changes of cells, we asked whether CAP and MSP300 could be involved in these processes as their functions have not yet been investigated in *Drosophila* heart. Orthologous genes, *SORBS* family and *Syne1* respectively, exhibit conserved cardiac expression in mammals (Banerjee et al., 2014; Dixon et al., 2015; Hong et al., 2014; Puckelwartz et al., 2010).

We first tested expression patterns of CAP and MSP300 by immunostaining and confirmed that they are both expressed in migrating CBs starting from late embryonic stage 13 (Fig. 1A-A"). CAP and MSP300 are co-expressed in a stereotyped punctate pattern on the apical and basal sides of each CB, clearly visible from stage 15 (Fig. 1B-B" and arrowheads in Fig. 1C-C"). This expression is maintained when the two rows of CBs have reached the dorsal midline (Fig. 1D-E"). While expression of CAP seems to be also diffuse under cell membranes (arrow in Fig 1E'), MSP300 is largely co-localized with CAP protein (arrowheads in Fig. 1E"). Transversal sections of 3D reconstructed, developing hearts confirmed co-localization of CAP and MSP300 on basal and apical sides of CBs in aorta as well as in the heart proper (arrows in Fig. 1F-F", Fig S1A, B). To validate CAP and MSP300 localization in the apical side of the luminal domain, we performed co-immunostaining experiments with CAP and Slit antibodies (Fig S1C-F"). We confirmed that CAP and MSP300 are enriched apically at the level of the lumen (arrowheads in Fig S1C-E) but absent at the CBs adhesion sites characterized by Armadillo expression (Fig. S1G, H). Unexpectedly, we also observed Slit localization in a punctate pattern at the basal side of CBs at stage 15-16, reminiscent of CAP and MSP300 expression patterns (arrows in Fig. S1C-C"). This dotty accumulation of Slit is transient as it becomes polarized at the luminal side at late stage 16 (Fig. S1F-F").

Next, we wondered whether CAP and MSP300 are interdependent for their punctate localization. MSP300 is a multidomain scaffold protein. Therefore, we hypothesized that it could participate in the recruitment and accumulation of CAP into subcellular compartments, creating a repeated punctate pattern. To test this, we performed an immunostaining in both

CAP and MSP300 mutants. We observed a clear loss of punctate accumulation of CAP on basal and apical CB sides in *MSP300*^{SZ75} mutant embryos, suggesting that MSP300 is required for CAP localization in CBs (arrows Fig 1G-H). Similarly, in *dCAP49e* mutants, the MSP300 expression pattern is severely affected. However, since some MSP300 expression in CBs persists, we conclude that CAP is only partially required for the MSP300 punctate pattern (arrows Fig 1 I-J). We also performed co-immunoprecipitation experiments using GFP-tagged MSP300 transgenic *Drosophila* line but couldn't find in our experimental conditions any interaction between MSP300-GFP and CAP indicating that several intermediate partners might be involved in the complex.

In summary, we observed that during the late phase of CBs migration, CAP, MSP300 and Slit co-localize in polarized dots on each side of CBs in the basal and luminal domains. These findings suggest that CAP and MSP300 are part of a protein complex as their punctate localization appears to be largely interdependent.

MSP300 and CAP are required for the correct alignment and number of Tin+ cardioblasts

We next examined *CAP* and *MSP300* functions during CBs migration. Immunostaining with antibodies against the muscle differentiation transcription factor Mef2, revealed misalignments of CBs in both *MSP300* and *CAP* mutants. (Fig. 2A-C"). Cardioblasts formed clusters (arrowheads in Fig. 2B,C) and multiple cell layers (brackets Fig. 2B,C). We scored these alignment defects and found that 80% of *MSP300* (44/55) and 64% of *CAP* mutant embryos (34/52) present a multilayered row of CBs suggesting that *MSP300* and *CAP* are both involved in maintaining cohesion of migrating CBs (Fig. 2K).

Slit and its Robo receptors are known factors in CB migration, alignment and polarization (MacMullin and Jacobs, 2006; Medioni et al., 2008; Qian et al., 2005; Santiago-Martinez et al., 2006). Slit/Robo mediated cardiac morphogenesis is modulated by the transmembrane integrin receptors, their ligands and intracellular interactors (Vanderploeg et al., 2012). Given the link between CAP and the integrin adhesion complex, as well as the observed alignment defects in *dCAP49e* embryos, we tested whether Slit localization is affected in *CAP* and *MSP300* mutants.

We found clear Slit localization defects in both mutants. (Fig. 2A-C"). Slit was ectopically expressed in misaligned CBs creating a meshwork between CBs (arrows in Fig. 2B',C'). Similar ectopic enrichment of Slit around mis-localized CBs has also been observed in cardiac specific knock-downs of *CAP* (miR strategy; Bharadwaj et al., 2013) and *MSP300* (short hairpin mediated strategy) (Fig. 2K, Fig. S2A-B"). Collectively, these data show that

CAP and MSP300 ensure correct Slit localization in CBs. They also suggest a potential interaction between CAP, MSP300 and the integrin complex in migrating CBs.

We then tested whether the CB cell shape is affected in *CAP* mutants. Alpha-spectrin staining, that marks cell membrane subdomain, showed that CAP^{49e} CBs are misarranged compared to the wild type (where CBs are perfectly aligned along AP axis and matching with their contralateral partner) (arrows and arrowheads in Fig. 2D). In CAP^{49e} hearts we observed changes in both the shapes and the orientation of CBs along the A-P axis (arrowhead in Fig. 2D'), CBs misalignment/matching defects (arrows and arrowheads, Fig. 2D,D') and mispositioning within rows of cells (star in Fig. 2D'), suggesting mis-regulation of CBs migration directionality.

We also tested the genetic interaction between *CAP* and *MSP300* using trans-heterozygous $dCAP49e/MSP300^{SZ75}$ mutant embryos. In contrast to single heterozygous control, CBs alignment is affected in trans-heterozygotes (18% versus 59%; Fig. 2K, Fig. S2C-C"), showing that *CAP* and *MSP300* genetically interact and play convergent roles during CBs migration. Finally, we checked whether changes in total cardiac cells number could account for *MSP300* and *CAP* mutant phenotypes. We performed immunostaining experiments using antibodies against H15 a transcription factor specific of all CBs and Seven-up (Svp) a marker of a CB subset giving rise to ostia. These two markers allow to distinguish the four Tin positive CBs (Svp-) from the two Svp positive CBs in each abdominal hemi-segment A2-A7. We found that knock out of either *MSP300* or *CAP* both lead to a significant increase in CBs number (Fig. 2E-J and L). Interestingly, only Tin-positive CBs were increased in homozygous mutant or cardiac specific KD of either *CAP* or *MSP300* suggesting a specific function of these genes in maintaining the post-mitotic state of Tin+ CBs (Fig. 2E-J, M, Fig. S5) thought to undergo symmetric cell divisions. Alignment defects also occur in hemi-segments without supernumerary CBs, but this appears to be concomitant with an increase in CBs in other hemi-segments. (arrows in Fig. 2G,H).

MSP300 is required for proper adult heart structure and function

Considering the impact of MSP300 loss of function on embryonic heart morphology and that $MSP300^{sz75}$ homozygous mutants are embryonic lethal, we wondered if cardiac specific KD of MSP300 could lead to some defects in the adult heart. We first validated the efficiency of MSP300 RNAi line in embryos by immunostaining (Fig. S3A-B') and analyzed semi-intact

preparations of the fly hearts to measure heart physiological parameters after KD using SOHA software (Ocorr et al., 2007).

MSP300 RNAi flies show a significant increase in systolic diameter leading to a reduction in fractional shortening (Fig. 3A,A'). MSP300 RNAi hearts stained for F-Actin show also disorganization and gaps (arrows in Fig. 3C') in the circumferential myofibrils by comparison to highly organized and densely packed myofibrils observed in control hearts (arrowheads in Fig. 3B'-C'). This disturbed cardiac architecture suggests a potential discontinuity in the arrangement of cardiomyocytes leading to failure in coordinated contraction.

Vinculin-Beta Integrin complex is required for CAP and MSP300 polarized localization

CAP protein interacts directly with Vinculin (Vinc) at the muscle attachment sites where it is recruited to the Integrin complex to modulate the Actin cytoskeleton (Bharadwaj et al., 2013). Therefore, we asked whether Vinc is also present in CBs during embryonic development and could be involved in CAP regulated processes. We took advantage of a recently generated Vinc-GFP knockin allele allowing us to follow Vinc localization *in vivo*. We detected restricted and similar Vinc-GFP signal at the apical and basal membranes of CBs consistent with CAP and MSP300 expression (arrows Fig. 4A-B"') as well as the localization of other integrin adhesion complex members such as βPS-integrin (arrows Fig. S4A-A"). Interestingly, we confirmed that this accumulation of Vinc coincides with F-Actin localization at basal (arrowheads Fig 4B-B"') and apical sides, revealed with Phalloidin staining (arrowheads Fig 4C-C'", Fig. S4B-B'").

To test whether Vinc is required for CAP localization, we analyzed the impact of heart-specific *Vinc* knockdown on both CAP and MSP300 expression (Fig. 4D-E"). We first validated the efficiency of *Vinc* KD by immunostaining in embryos (Fig. S3C-D') and observed that the heart proper morphology contains inclusion of CBs (Fig. 4E, arrowhead) indicating their misalignment during migration. Dots of co-accumulation of CAP and MSP300 are still present, however their pattern is disorganized, suggesting that polarization of CBs is defective (arrows Fig. 4E-E"). Cardiac specific KD of *Vinc* also induces a meshwork of Slit (Fig. 4F-F") and an increase in Tin CBs number in some hemi-segments, which is consistent with CAP and MSP300 loss of function (Fig. 5A-D, and Fig. 5G-I). Similar results are also obtained in cardiac specific KD of *βPS-integrin* (Fig. 5E, and Fig. 5G-I). Interestingly, transheterozygous mutant embryos with *MSP300sz75* combined with cardiac alpha PS3 integrin Scb^{01288} show disorganized CB alignment and increased number of Tin

CBs (Fig. 5F) showing their involvement in the same pathway. These results are reminiscent of the genetic interaction recently identified between *CAP* and *Scb* (Jammrath et al., 2020) suggesting related roles of CAP, MSP300 and Integrin complex in controlling post-mitotic state of Tin CBs. Finally, we tested if the Integrin ligand Laminin A, also known to interact genetically with *slit* (MacMullin and Jacobs, 2006), is affected in the loss of *MSP300, Vinc* and *βPS-integrin.* Interestingly, we observed a disorganized pattern of LamA in *MSP300* homozygous mutant embryos with breaks in the apical side and the basal lamina, suggesting that Nesprin-like proteins are required for ECM structure (Fig. 6A-B'). These results are consistent with defects in LamA pattern observed after *Vinc* and *βPS-integrin* KD (Fig. 6A"-B'"). A similar requirement of MSP300 and Integrin complex was also observed for the correct localization of another ECM component Perlecan (Trol) a secreted heparan sulfate proteoglycan (Fig. 6C-D"').

Overall, the polarized location of the CAP-MSP300-Vinc / Integrin complexes plays an important role in determining the appropriate number and arrangement of CBs and the localization of ECM proteins.

CAP and MSP300 mediate F-actin bridging between nucleus and integrin complex

One possibility is that CAP and MSP300 function by locally binding Vinc adhesion complexes to the actin cytoskeleton and the nucleus. This would generate a directional internal tension which would keep the CBs polarized, maintain their post-mitotic state and their alignment and would thus allow correct lumen formation and compaction of the heart tube. MSP300/Syne 1-2 proteins contain an actin binding domain, while CAP binds to actin-binding proteins including Vinc. This suggests that F-actin might be a potential co-partner associated to the MSP300-CAP-Vinc dots during CB migration. To confirm the involvement of F-Actin in bridging the nucleus to the integrin complex, we analyzed null mutation and cardiac specific KD of WASp. WASp regulates the nucleation activity of the Arp2/3 complex, facilitating the assembly of branched actin filament networks with the spatiotemporal control required to orchestrate cellular processes (Padrick et al., 2011).

Consistent with our previous findings, cardiac (Hand-GAL4) or Tin CBs specific KD of WASp lead to defects in alignment of cardiac cells and increased number of Tin CBs in some hemi-segments (Fig. 7A-D, Fig. 7F-H and Fig. S5). These defective arrangements of CBs also occur in hemi-segments bearing the correct number of Tin CBs (arrows in Figure 7D) suggesting that clustering could occur as a consequence of exiting the post-mitotic state of

CBs in a different hemi-segment. Finally, we assessed the genetic interaction between *MSP300* and *WASP* by comparing single heterozygous mutant for each gene with the transheterozygous context. Our results clearly demonstrate a significant increase in CBs alignment defects and Tin CBs number in transheterozygous embryos suggesting that *MSP300* and *WASp* function in a similar pathway during heart closure to regulate actin dynamics (Fig. 7E, and Fig. 7F-H). Interestingly, removing WASp function had a similar negative impact on ECM proteins LamA and Trol localization than *MSP300* and Integrin complex loss of function (Fig. 6A""-D"") strengthening their involvement in the same mechanism.

To further confirm the link between F-actin and MSP300 localization, we performed Phalloidin staining to reveal the F-actin pattern in migrating CBs. Interestingly, F-actin accumulates on basal and apical sides of CBs very much like CAP and MSP300 (Fig. 8A-A"' and Fig. S2B-B"'). Hence, we tested whether MSP300 was required to stabilize F-actin accumulation at the interface of nucleus and the CAP-Focal adhesion complex. Indeed, MSP300 loss of function induced a strong decrease in localized F-actin expression in CBs (arrowheads Fig. 8B, C and Fig. 8D). Strikingly, this F-actin phenotype was stronger for Tin positive CBs, as Svp-CBs still accumulated F-actin in MSP300 mutants (arrows Fig. 8B,C) suggesting a specific function of MSP300 in Tin-CBs.

Consistent with its known function, *WASp*^{3} mutant embryos show a significant reduction of F-Actin level in a similar manner than in *MSP300* mutant hearts (Fig. 8D).

Taken together, these data suggest that CAP and MSP300 control CBs cell cycle exit and alignment by facilitating a F-actin linkage of the nucleus with the CB cell membrane. This function is limited during migration to the "leading CBs" population expressing Tin.

F-actin stress fibers have been shown to exert mechanical tension on the nucleus, providing mechano-sensing properties to orient the nucleus and modulate its shape during cell migration. Thus, we measured nucleus shape in *CAP* and *MSP300* mutants. We observed that *CAP* and *MSP300* null mutants or cardiac specific CAP KD induce a significant decrease of nuclei volume as well as an increase in flatness relative to controls (Fig. 9A,B). Consistent with our findings, *WASp*^{3} mutant embryos show the same effect on nuclei shape suggesting the requirement of actin stress fibers to maintain nuclei morphology during CBs migration.

Discussion

In this study, we have analyzed expression and function of two novel actors of cardiac morphogenesis: CAP, an integrin complex adaptor protein and MSP300, a Nesprin protein belonging to the LINC complex. Our study highlights a crucial role for CAP and MSP300 in maintaining the nucleus-cell membrane connection via the integrin/vinculin adhesion complex, which is ultimately required in locking cell divisions processes during the migration progression of Tin positive cardiomyocytes. (Fig. 8C). We also provide evidence that this nucleus-cytoskeleton-cell membrane link is important to maintain CB polarity, contact between ipsilateral and contralateral CBs and for maintaining proper nucleus shape.

These mechanisms appear to be coupled and more work will be needed to determine whether the quiescent stage exit is a cause or a consequence of polarity and alignment defects. Slit localization is also affected in *MSP300* and *CAP* mutants, suggesting that Slit mediated-directionality of CBs migration might be affected. Indeed, a conserved aspect of Slit/Robo signaling is its involvement in cell guidance mechanisms (Fish et al., 2011; Raza and Jacobs, 2016; Wu et al., 1999). In *Drosophila*, Slit is known to interact genetically with several members of the integrin complex (αPS3, βPS) and the integrins are required for apical localization of Slit and leading-edge activity. The direct coupling between the cell membrane and the ECM at integrin-based adhesion sites (focal adhesion) allows cells to mechanically sense their physical environment and tune downstream signaling events that regulate the organization of the cytoskeleton. Vinculin is a key player in focal adhesion where it interacts directly with Talin and ensures a link between adhesion proteins and actin cytoskeleton (Burridge and Mangeat, 1984; Humphries et al., 2007; Rothenberg et al., 2018). In Vertebrates and in *Drosophila*, CAP has the potential to directly interact with Vinculin (Bharadwaj et al., 2013). In CBs, loss of Vinculin leads to disorganized CAP and MSP300 dotty localization, probably due to the loss of Vinc-anchoring points at the cell membrane, resulting in affected CBs number, polarity and motility. We propose that MSP300 and CAP ensure the connection of nuclei to adhesion complex via actin cytoskeleton and Vinculin and could thus modulate the coordination between cell division arrest and the initiation of migration. However, even though both rows of CBs appear to reach the dorsal midline in *CAP* and *MSP300* mutant embryos, their expression pattern, maintained throughout cardiac tube formation, could suggest a potential secondary function in fine regulation of the dynamics of CBs migration.

MSP300 possesses spectrin repeats allowing interaction with actin. In this study, we demonstrate the genetic interaction of *MSP300* with *CAP* and *WASp* an activator of Arp2/3 complex suggesting that branched actin network is involved in connecting the nucleus to the cell membrane (Padrick et al., 2011).

Transition from cell cycle exit to cell migration is a coordinated process that requires multilevel controls in terms of cell polarity, cell adhesion and differentiation involving changes in gene expression programs. LINC complexes are known to be important in transmitting mechanical stresses from the cytoskeleton to the inside of the nucleus that ultimately leads to changes in nuclear structure and organization and regulates cell cycle progression (Uroz et al., 2018). Recently, the LINC complex has been shown to transmit the forces from the ß1integrin-engaged actin network to the nuclear lamina to directly regulate the expression of epidermal differentiation genes (Carley et al., 2021). Our results support these views although the outcome may depend on the context. One of our interesting observations is that CAP-MSP300 dots accumulate at both sides of migrating CBs. Recent evidences suggest the existence of an actin structure called perinuclear actin-cap that interact with specific actin-cap-associated focal adhesion components at two positions in the direction of the aligned actin-cap fibers, at leading lamellipodial edge and the trailing edge of the cell. This newly identified actin structure is linked to the nucleus via the LINC complex (Kim et al., 2012; Maninova et al., 2017) and might be necessary to coordinate quiescence, cell polarity and nucleus shape during migration. Furthermore, nuclei deformations observed in *CAP*, *MSP300* and *WASp* mutant nuclei are reminiscent of a previously described model based on results obtained after Nesprin-1 siRNA treatment of endothelial cells (Anno et al., 2012). Indeed, like in Nesprin-1 KD, CBs nuclei seem more sensitive to deformation and become smaller and flattened suggesting that WT nuclei might be subjected to directional tensile forces along the apical-basal axis during CBs migration.

Additional work will determine if F-actin bound to the nucleus through MSP300 and to focal adhesion leads to sustainable force transmission to CBs nuclei and whether direct transmission of mechanical force to the nucleus can influence the exit of CBs from the cell cycle. Recent findings have shown that *nesprin-1* mutations lead to increased activation of the ERK pathway in mouse heart tissue (Zhou et al., 2017). In vertebrate CAP/Ponsin has been also shown to repress MAPK pathway (Zhang et al., 2006). In *Drosophila*, late EGFR mediated ERK activation has been shown to promote Tin CBs subpopulation (Schwarz et al., 2018). According to our data, one hypothesis is that CAP and MSP300 would counteract EGF pathway maintaining the correct number of Tin migrating CBs. Further investigations will be

needed to clarify the involvement of CAP, F-actin and MSP300 in controlling these processes.

Our physiological analysis of *MSP300* mutant adult hearts indicate that the cardiac contractile function is affected. Fractional shortening in adults were strongly affected in *MSP300* KD and linked to locally defective morphology of adult hearts.

During the process of publication of our results a new study has shown that a similar phenotype occurs following CAP mutation in larvae and adult heart (Jammrath et al., 2020) suggesting that MSP300-CAP connection might be conserved for the correct architecture and function in the adult heart. These preliminary results open new perspectives concerning a possible implication of this connection in the formation of the primitive cardiac tube of vertebrates.

Materials and methods

Drosophila genetics

Drosophila CAP deletion mutant *dCAP49e* deletes 2.9kb downstream of $CAP^{CA06924}$ P-element. The *dCAP49e* mutant and *UAS-CAPmiR* construct has been generated according to (Bharadwaj et al., 2013). *dCAP49e, P(UAS-CAP.miRNA)3* were from Bloomington Stock Center. $MSP300^{SZ75}$ mutant is a gift from Talila Volk (Weizmann Institute of Science, Rehovot, Israel). It carries truncation of the C-terminal part of MSP300 (Rosenberg-Hasson et al., 1996). MSP300 TRIP lines (32377, 32848) myospheroid TRIP lines (27735, 33642), WASp TRIP lines (25955, 36647) and Scb^{01288} mutant line (11035) and EGFP-MSP300 protein trap (59757) from Bloomington Stock Center. Vinculin RNAi lines (v34585, v34586; Kaushik et al., 2015) were obtained from the Vienna *Drosophila* Research Center. Vinculin-GFP line is tagged at its N-terminus with superfolded GFP using a pFlyFos025866 Fosmid which encompasses the 8 kb of Vinculin gene along with 23.4 kb upstream and 6.8 kb downstream regions integrated in attp2 site (Kale et al., 2018). Cardiac GAL4 drivers used in this study are $Hand^{4.2}$ and TinC Δ4.

Immunostaining

Drosophila embryos were processed for immunostaining as described previously for most of the experiments (Patel, 1994). Heat fixation were also performed on WT dechorionated embryos for 10 second in boiling water followed by 5 min devitellinization in a 1:1 mix of heptan and methanol on shaker. Microscopic observations were performed by confocal microscopy to produce images using Leica SP8. All images were acquired using a 40× oil objective with a numerical aperture of 1.3. The following antibodies were used: Rabbit anti-CAP 1:1000 (a gift from A.L Kolodkin, Johns Hopkins University School of Medicine, Baltimore, USA; Bharadwaj et al., 2013), Rabbit anti-Mef2 1:1000 (a gift from M.V Taylor, School of Biosciences, Cardiff University, Cardiff, UK), Guinea Pig anti-MSP300 1:2000 (Rosenberg-Hasson et al., 1996) and Guinea Pig anti-Laminin A 1:1000 (a gift from T. Volk, Weizmann Institute of Science, Rehovot, Israel), Guinea Pig anti-H15 1:2000 (a gift from J.B

Skeath Washington University School of Medicine, St. Louis, USA), Rabbit anti-Trol 1:1000 (a gift from S. Baumgartner Lund University, Lund, Sweden) mouse anti-Slit at 1:100 (DSHB), anti-Seven up at 1:100 (DSHB), anti-Armadillo at 1:100 (DSHB), anti-α-Spectrin 1:100 (DSHB), anti-Vinculin 1:50 (Santa Cruz N-19), Alexa fluor 488 Phalloidin 1:300 (Invitrogen A12379).

Optical cross section of *Drosophila* embryonic heart tubes

IMARIS software 7.6.5 has been used to open images in a 2D display mode (Slice view).
In the menu bar we selected "Edit – Crop 3D". A rectangle, with yellow borders, will overlay on all three views. It represents the region of interest and it can be modified in size and position resulting in the cross-sections of the selected part of the heart tube.
The Surpass mode is used to create a 3D reconstruction of the *Drosophila* embryonic heart tubes, and setting the pointer on Navigate mode allows to rotate the resulting object through a range of angles. This was done in two different regions: aorta and the heart proper.

***Drosophila* Heart Physiology**

Semi-intact preparations of the fly hearts were made as described previously (Ocorr 2009). Female flies are used for technical reasons (females are bigger). Briefly, flies (20 each genotype) were dissected in oxygenated artificial hemolymph (AHL) to expose the linear tube-like heart. Following 15-20 minutes of recovery in fresh oxygenated AHL, 30-second high-speed movies (~140 fps) of contracting hearts were captured with a 10x immersion objective. These movies were analyzed with the SOHA software (sohasoftware.com, Ocorr et al. 2007, 2009, Fink 2009). The following key heart function parameters were measured: Diastolic Interval (DI), Systolic Interval (SI), Diastolic Diameter (DD), and Systolic Diameter (SD). Functional parameters were calculated based on these measures including: Heart Period (HP, DI+SI). Fractional Shortening (FS) as a measure of contractility was calculated as FS= [(EDD-ESD)/EDD], where EDD is the DD and ESD is the SD.

F-actin quantification

F-actin was detected and quantified using the Weka segmentation tool in ImageJ in both heart proper and aorta in each embryo. The same classifier has been used on every image. The values have been normalized on the total area of the heart.

Nuclei morphology measurement

Microscopic observations were performed by confocal microscopy to produce images using Leica SP8. All images were acquired using a 40× oil objective with a numerical aperture of 1.3, a pixel size of 0.054 µm (x,y) and voxel depth of 0.2 µm. Furthermore, all initial anisotropic voxels are converted to isotropic voxel (i.e. cubic, xyz=0.1 µm) prior to calculation. The ImageJ plugin NucleusJ was used to characterize nuclear morphology (Dubos et al., 2020; Poulet et al., 2015). A detailed description of the quantitative parameters generated by NucleusJ can be found in supplemental materials of Poulet et al. (Poulet et al., 2015).

Quantification and statistical analysis

Statistical analyses were performed using Xlstat.
The significance of the difference was determined using unpaired Wilcoxon-Mann–Whitney tests. All p-values are two tailed. P value <0.05 were considered significant.

Acknowledgements

We thank Sophie Desset, Tristan Dubos and Caroline Vachias (GReD institute) for their technical assistance as well as CLIC facility.

Competing interests

The authors declare no competing financial interests.

Funding

This work was supported by Agence Nationale de la Recherche JC (CARDIAC-SPE), FEDER/Region Auvergne Young Researcher, TEFOR-ANR Infrastructure and CAP-2025 ISITE challenge-3 grants.

References

Anno, T., Sakamoto, N., and Sato, M. (2012). Role of nesprin-1 in nuclear deformation in endothelial cells under static and uniaxial stretching conditions. *Biochemical and biophysical research communications* **424**, 94-99.

Banerjee, I., Zhang, J., Moore-Morris, T., Pfeiffer, E., Buchholz, K. S., Liu, A., Ouyang, K., Stroud, M. J., Gerace, L., Evans, S. M., et al. (2014). Targeted ablation of nesprin 1 and nesprin 2 from murine myocardium results in cardiomyopathy, altered nuclear morphology and inhibition of the biomechanical gene response. *PLoS genetics* **10**, e1004114.

Bharadwaj, R., Roy, M., Ohyama, T., Sivan-Loukianova, E., Delannoy, M., Lloyd, T. E., Zlatic, M., Eberl, D. F. and Kolodkin, A. L. (2013). Cbl-associated protein regulates assembly and function of two tension-sensing structures in Drosophila. *Development* **140**, 627-638.

Biersmith, B., Wang, Z. H. and Geisbrecht, E. R. (2015). Fine-Tuning of the Actin Cytoskeleton and Cell Adhesion During Drosophila Development by the Unconventional Guanine Nucleotide Exchange Factors Myoblast City and Sponge. *Genetics* **200**, 551-567.

Bryantsev, A. L. and Cripps, R. M. (2009). Cardiac gene regulatory networks in Drosophila. *Biochim Biophys Acta* **1789**, 343-353.

Burridge, K. and Mangeat, P. (1984). An interaction between vinculin and talin. *Nature* **308**, 744-746.

Busser, B. W., Haimovich, J., Huang, D., Ovcharenko, I. and Michelson, A. M. (2015). Enhancer modeling uncovers transcriptional signatures of individual cardiac cell states in Drosophila. *Nucleic acids research* **43**, 1726-1739.

Carley, E., Stewart, R.M., Zieman, A., Jalilian, I., King, D.E., Zubek, A., Lin, S., Horsley, V. and King, M.C. (2021). The LINC complex transmits integrin-dependent tension to the nuclear lamina and represses epidermal differentiation. *eLife* **10**:e58541

Dixon, D. M., Choi, J., El-Ghazali, A., Park, S. Y., Roos, K. P., Jordan, M. C., Fishbein, M. C., Comai, L. and Reddy, S. (2015). Loss of muscleblind-like 1 results in cardiac pathology and persistence of embryonic splice isoforms. *Scientific reports* **5**, 9042.

Dubos, T., Poulet, A., Gonthier-Gueret, C., Mougeot, G., Vanrobays, E., Li, Y., Tutois, S., Pery, E., Chausse, F., Probst, A.V., Tatout, C. and Desset, S. (2020) Automated 3D bio-imaging analysis of nuclear organization by NucleusJ 2.0. *Nucleus* **11**, 315-329

Fink, M., Callol-Massot, C., Chu, A., Ruiz-Lozano, P., Belmonte, J.C.I,., Giles, W., Bodmer, R., Ocorr, K. (2009). A new method for detection and quantification of heartbeat parameters in Drosophila, zebrafish, and embryonic mouse hearts. *Biotechniques* **46**, 101-113

Fish, J. E., Wythe, J. D., Xiao, T., Bruneau, B. G., Stainier, D. Y., Srivastava, D. and Woo, S. (2011). A Slit/miR-218/Robo regulatory loop is required during heart tube formation in zebrafish. *Development* **138**, 1409-1419.

Friedl, P., Wolf, K. and Lammerding, J. (2011). Nuclear mechanics during cell migration. *Current opinion in cell biology* **23**, 55-64.

Fruleux, A. and Hawkins, R. J. (2016). Physical role for the nucleus in cell migration. *Journal of physics. Condensed matter : an Institute of Physics journal* **28**, 363002.

Haack, T., Schneider, M., Schwendele, B. and Renault, A. D. (2014). Drosophila heart cell movement to the midline occurs through both cell autonomous migration and dorsal closure. *Developmental biology* **396**, 169-182.

Haag, T. A., Haag, N. P., Lekven, A. C. and Hartenstein, V. (1999). The role of cell adhesion molecules in Drosophila heart morphogenesis: faint sausage, shotgun/DE-cadherin, and laminin A are required for discrete stages in heart development. *Developmental biology* **208**, 56-69.

Hong, S. E., Song, H. K. and Kim, D. H. (2014). Identification of tissue-enriched novel transcripts and novel exons in mice. *BMC genomics* **15**, 592.

Humphries, J.D., Wang, P., Streuli, C., Geiger, B., Humphries, M.J., Ballestrem, C. (2007). Vinculin controls focal adhesion formation by direct interactions with talin and actin. *Journal of cellular biology* **179**, 1043-1057.

Ichikawa, T., Kita, M., Matsui, T. S., Nagasato, A. I., Araki, T., Chiang, S. H., Sezaki, T., Kimura, Y., Ueda, K., Deguchi, S., et al. (2017). Vinexin family (SORBS) proteins play different roles in stiffness-sensing and contractile force generation. *Journal of cell science* **130**, 3517-3531.

Jammrath, J., Reim, I., Saumweber, H. (2020). Cbl-Associated Protein CAP contributes to correct formation and robust function of the Drosophila heart tube. *PLoS one* **15**, e0233719.

Jin, H., Stojnic, R., Adryan, B., Ozdemir, A., Stathopoulos, A. and Frasch, M. (2013). Genome-wide screens for in vivo Tinman binding sites identify cardiac enhancers with diverse functional architectures. *PLoS genetics* **9**, e1003195.

Junion, G., Spivakov, M., Girardot, C., Braun, M., Gustafson, E. H., Birney, E. and Furlong, E. E. (2012). A transcription factor collective defines cardiac cell fate and reflects lineage history. *Cell* **148**, 473-486.

Kale, G. R., Yang, X., Philippe, J. M., Mani, M., Lenne, P. F. and Lecuit, T. (2018). Distinct contributions of tensile and shear stress on E-cadherin levels during morphogenesis. *Nature communications* **9**, 5021.

Kaushik, G., Spenlehauer, A., Sessions, A.O., Trujillo, A.S., Fuhrmann, A., Fu, Z., Venkatraman, V., Pohl, D., Tuler, J., Wang, M., et al. (2015). Vinculin network-mediated cytoskeletal remodeling regulates contractile function in the aging heart. *Science Translational Medicine* **7**, 292-299.

Kim, D. H., Khatau, S. B., Feng, Y., Walcott, S., Sun, S. X., Longmore, G. D. and Wirtz, D. (2012). Actin cap associated focal adhesions and their distinct role in cellular mechanosensing. *Scientific reports* **2**, 555.

Lovato, T. L. and Cripps, R. M. (2016). Regulatory Networks that Direct the Development of Specialized Cell Types in the Drosophila Heart. *Journal of cardiovascular development and disease* **3**.

MacMullin, A. and Jacobs, J. R. (2006). Slit coordinates cardiac morphogenesis in Drosophila. *Developmental biology* **293**, 154-164.

Maninova, M., Caslavsky, J. and Vomastek, T. (2017). The assembly and function of perinuclear actin cap in migrating cells. *Protoplasma* **254**, 1207-1218.

Medioni, C., Astier, M., Zmojdzian, M., Jagla, K. and Semeriva, M. (2008). Genetic control of cell morphogenesis during Drosophila melanogaster cardiac tube formation. *The Journal of cell biology* **182**, 249-261.

Mellad, J.A, Waren, D.T., Shanahan, C.M. (2011). Nesprins LINC the nucleus and cytoskeleton. *Current opinion cell biology* **23**, 47-54.

Ocorr, K., Reeves, N.L, Wessells, R.J., Fink, M., Chen, H.S.V., Akasaka, T., Yasuda, S., Metzger, J.M., Giles, W., et al. (2007). KCNQ potassium channel mutations cause cardiac arrhythmias in Drosophila that mimic the effects of aging. *Proceedings of the National Academy of Sciences of the United States of America* **104**, 3943-3948.

Padrick, S.B., Doolittle, L.K., Brautigam, C.A., King, D.S. and Rosen, M.K. (2011). Arp2/3 complex is bound and activated by two WASP proteins. *Proceedings of the National Academy of Sciences of the United States of America* **108**, 472-479

Patel, N. H. (1994). Imaging neuronal subsets and other cell types in whole-mount Drosophila embryos and larvae using antibody probes. *Methods in cell biology* **44**, 445-487.

Poulet, A., Arganda-Carreras, I., Legland, D., Probst, A. V., Andrey, P. and Tatout, C. (2015). NucleusJ: an ImageJ plugin for quantifying 3D images of interphase nuclei. *Bioinformatics* **31**, 1144-1146.

Puckelwartz, M. J., Kessler, E. J., Kim, G., Dewitt, M. M., Zhang, Y., Earley, J. U., Depreux, F. F., Holaska, J., Mewborn, S. K., Pytel, P., et al. (2010). Nesprin-1 mutations in human and murine cardiomyopathy. *Journal of molecular and cellular cardiology* **48**, 600-608.

Qian, L., Liu, J. and Bodmer, R. (2005). Slit and Robo control cardiac cell polarity and morphogenesis. *Current biology : CB* **15**, 2271-2278.

Raza, Q. and Jacobs, J. R. (2016). Guidance signalling regulates leading edge behaviour during collective cell migration of cardiac cells in Drosophila. *Developmental biology* **419**, 285-297.

Rosenberg-Hasson, Y., Renert-Pasca, M. and Volk, T. (1996). A Drosophila dystrophin-related protein, MSP-300, is required for embryonic muscle morphogenesis. *Mechanisms of development* **60**, 83-94.

Rothenberg, K. E., Scott, D. W., Christoforou, N. and Hoffman, B. D. (2018). Vinculin Force-Sensitive Dynamics at Focal Adhesions Enable Effective Directed Cell Migration. *Biophysical journal* **114**, 1680-1694.

Rugendorff, A., Younossi-Hartenstein, A. and Hartenstein, V. (1994). Embryonic origin and differentiation of the Drosophila heart. *Roux's archives of developmental biology : the official organ of the EDBO* **203**, 266-280.

Santiago-Martinez, E., Soplop, N. H. and Kramer, S. G. (2006). Lateral positioning at the dorsal midline: Slit and Roundabout receptors guide Drosophila heart cell migration. *Proceedings of the National Academy of Sciences of the United States of America* **103**, 12441-12446.

Stark, K. A., Yee, G. H., Roote, C. E., Williams, E. L., Zusman, S. and Hynes, R. O. (1997). A novel alpha integrin subunit associates with betaPS and functions in tissue morphogenesis and movement during Drosophila development. *Development* **124**, 4583-4594.

Swope, D., Kramer, J., King, T. R., Cheng, Y. S. and Kramer, S. G. (2014). Cdc42 is required in a genetically distinct subset of cardiac cells during Drosophila dorsal vessel closure. *Developmental biology* **392**, 221-232.

Uroz, M., Wistorf, S., Serrra-Picamal, X., Conte, V., Sales-Pardo, M., Roca-Cusachs, P., Guimera, R. and Trepat, X. (2018). Regulation of cell-cycle progression by cell-cell and cell-matrix forces. *Nature Cell Biology* **20,** 646-654.

Vanderploeg, J. and Jacobs, J. R. (2015). Talin is required to position and expand the luminal domain of the Drosophila heart tube. *Developmental biology* **405**, 189-201.

Vanderploeg, J., Vazquez Paz, L. L., MacMullin, A. and Jacobs, J. R. (2012). Integrins are required for cardioblast polarisation in Drosophila. *BMC developmental biology* **12**, 8.

Vogler, G., Liu, J., Iafe, T. W., Migh, E., Mihaly, J. and Bodmer, R. (2014). Cdc42 and formin activity control non-muscle myosin dynamics during Drosophila heart morphogenesis. *The Journal of cell biology* **206**, 909-922.

Vogler, G. and Ocorr, K. (2009). Visualizing the beating heart in Drosophila. *Journal of visualized experiments* **31**, 1425.

Wang, J., Tao, Y., Reim, I., Gajewski, K., Frasch, M. and Schulz, R. A. (2005). Expression, regulation, and requirement of the toll transmembrane protein during dorsal vessel formation in Drosophila melanogaster. *Molecular and cellular biology* **25**, 4200-4210.

Wang, S., Reuveny, A. and Volk, T. (2015). Nesprin provides elastic properties to muscle nuclei by cooperating with spectraplakin and EB1. *The Journal of cell biology* **209**, 529-538.

Wu, W., Wong, K., Chen, J., Jiang, Z., Dupuis, S., Wu, J. Y. and Rao, Y. (1999). Directional guidance of neuronal migration in the olfactory system by the protein Slit. *Nature* **400**, 331-336.

Zhang, S., Amourda, C., Garfield, D. and Saunders, T. E. (2018). Selective filopodia adhesion ensures robust cell matching in the Drosophila heart. *Developmental Cell*. **46**, 189-203.

Zhang, M., Liu, J., Cheng, A., DeYoung, S.M., Chen, X., Dold, L.H., Saltiel, A.R. (2006). CAP interacts with cytoskeletal proteins and regulates adhesion-mediated ERK activation and motility. *EMBO Journal* **25**, 5284-5293.

Zhou, C., Li, C., Zhou, B., Sun, H., Koullourou, V., Holt, I., Puckelwartz, M. J., Warren, D. T., Hayward, R., Lin, Z., et al. (2017). Novel nesprin-1 mutations associated with dilated cardiomyopathy cause nuclear envelope disruption and defects in myogenesis. *Human molecular genetics* **26**, 2258-2276.

Figures

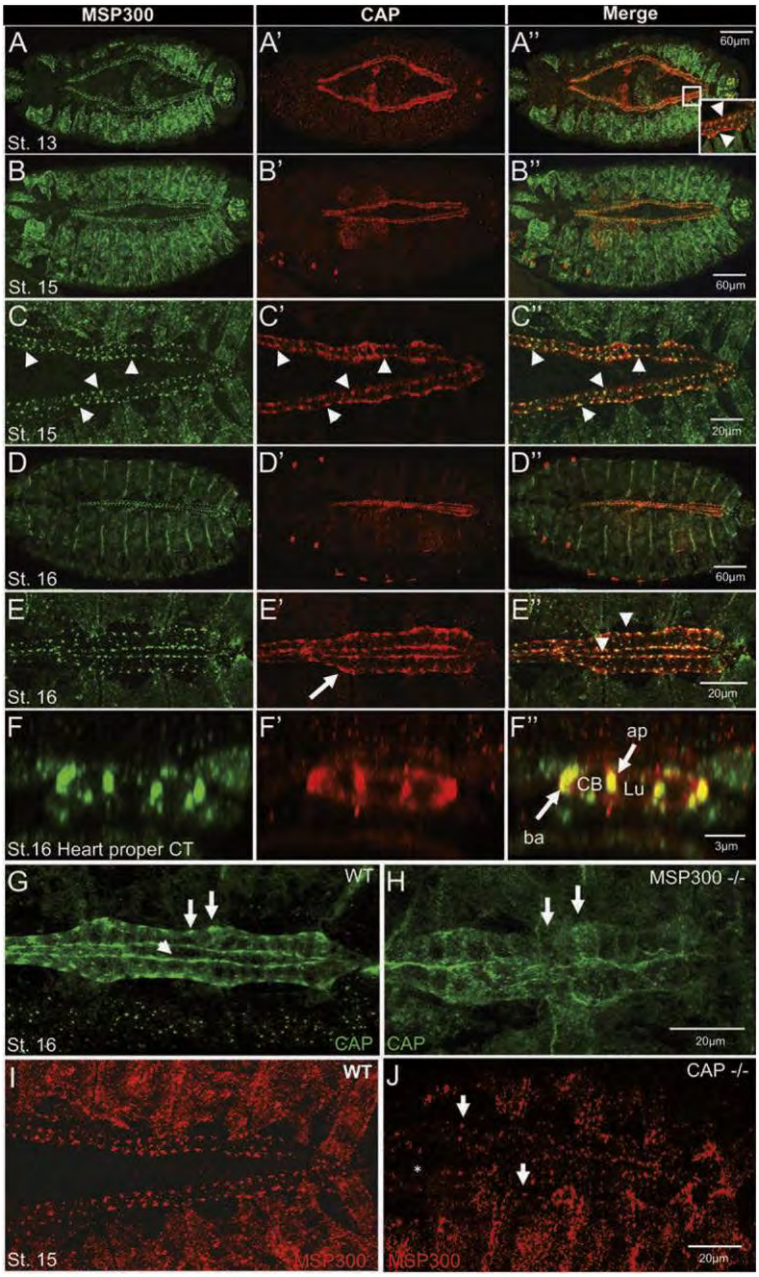

Figure 1: CAP and MSP300 colocalize in CBs on basal and apical dots inter-dependently
(A-A") Dorsal view of a late stage 13 embryo showing by immunostaining with anti-CAP and anti-MSP300 antibodies co-expression in cardioblasts.
(B-B") Dorsal view of an early stage 15 embryo showing that CAP and MSP300 accumulate in dots on the basal and apical sides of cardioblasts.
(C-C") Higher magnification showing that MSP300 accumulates where the maximum of CAP proteins on apical and basal sides (arrowheads) is present.
(D-D") Dorsal view of a stage 16 embryo showing that CAP and MSP300 punctate pattern is present until the stage of lumen formation. We observe also a colocalization in muscle attachment sites at segmental borders.

(E-E”) Higher magnification showing that CAP accumulation is extended under the cell membrane (arrow) and that CAP and MSP300 colocalize on basal and luminal sides.
(F-F”) 3D reconstruction of transversal cut in heart proper validating accumulation of MSP300 and CAP on basal and apical side of CBs (ba: basal side, ap: apical side, Lu: lumen, CB: cardioblast).
(G-H) Dorsal view of a stage 16 embryo showing that loss of MSP300 induces a strong decrease in CAP localization on basal (arrows) and apical sides (arrowhead).
(I-J) Dorsal view of a stage 15 embryo showing that loss of CAP leads to a partial reduction of MSP300 dotty pattern. Some dots are still visible in few CBs (arrows).

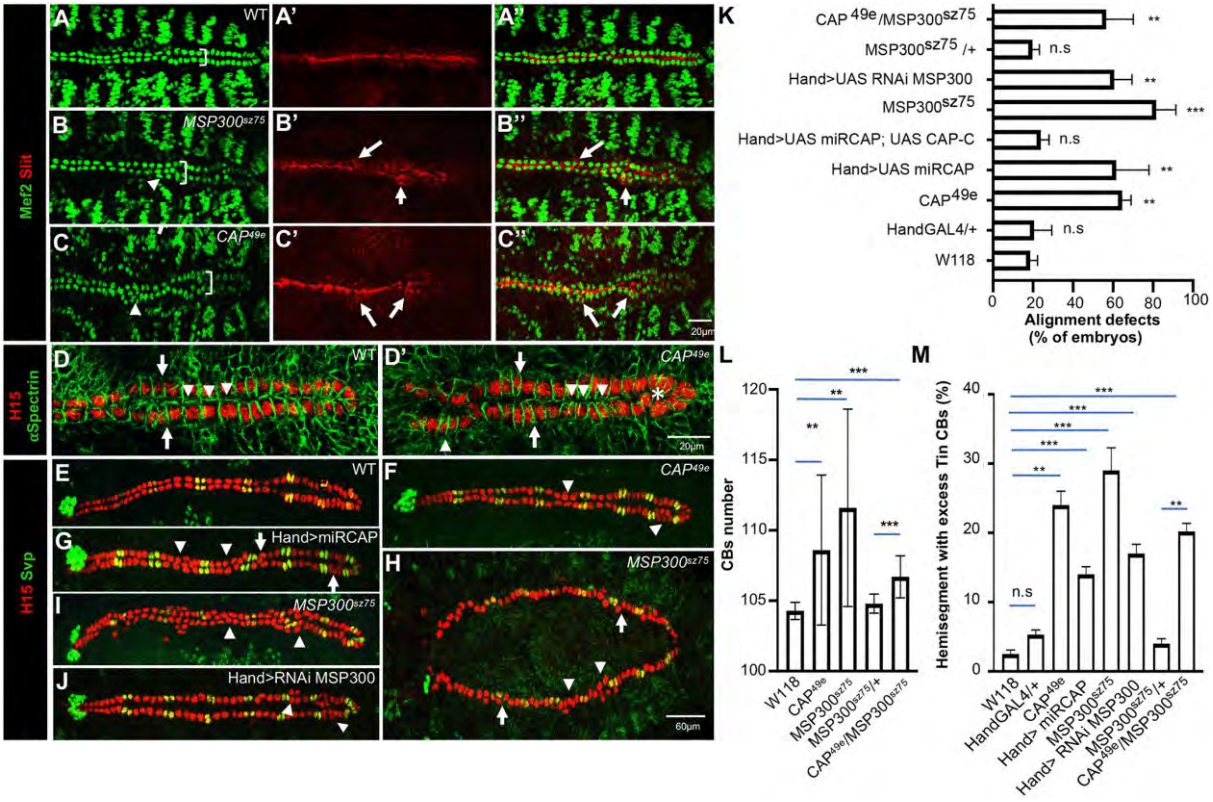

Figure 2: MSP300 and CAP are required for correct CBs alignment and number during migration

(A-C") Dorsal view of stage 16 embryos showing that compared to WT, the loss of MSP300 and CAP induces alignment defects visible with CBs nuclear marker Mef2 and CB polarity marker Slit. A-A" show the WT context with 2 rows of CBs (bracket) and apically localized Slit protein. B-B" In loss of *MSP300* more than 2 rows of CBs are visible in some segments (bracket) and Slit pattern is not polarized with some accumulation visible on lateral and basal side of CBs. C-C" *CAP49e* mutant embryos show similar phenotypes than the loss of *MSP300*.

(D-D') Cell membrane marker α-Spectrin shows that in *CAP49e* mutant cells are misaligned, and matching between contralateral CBs is disturbed (compare arrows in D and D') impacting contacts between CBs (compare arrowheads in D and D'). Mis-localized cells are also visible in *CAP* mutant (star).

(E-G and I, J) Dorsal view of stage 16 embryos revealing specifically with anti-H15 antibody all cardiomyocytes including Svp ostia cells stained with anti-Svp. *CAP49e* and *MSP300sz75* homozygous mutants as well as cardiac specific knock down for these two genes induce an increase in Tin CBs number in some hemi-segments (arrowheads) while Svp CBs number remain unchanged. Arrows point hemi-segments with correct CBs number but bearing alignment defects.

(H) Dorsal view of stage 14 embryos revealing uncoordinated CBs migration in *MSP300sz75* homozygous mutants in hemi-segments with (arrowheads) or without (arrows) increase in Tin CBs number.

(K) Bar chart showing the percentage of embryos with CB alignment defects (CAP49e n=52, MSP300 n=55 and for all other genotypes n=30) Error bars represent SD; two-tailed pvalues were calculated using a Wilcoxon-Mann Whitney test, pval< 0,0001(***).

(L) Bar chart showing quantification of the mean CBs number in mentioned genetic backgrounds (n=30) Error bars represent SD; two-tailed pvalues were calculated using a Wilcoxon-Mann Whitney test, pval< 0,0001(***).
(M) Bar chart showing the percentage of hemi-segments with supernumerary Tin CBs. (W118 n=240, *CAP49e* n=360, Hand>miRCAP n=240, *MSP300sz75* n=360, Hand>RNAi MSP300 n=240, *MSP300sz75/+* n= 240, *MSP300sz75/CAP49e* n=240). Error bars represent SD; two-tailed pvalues were calculated using a Wilcoxon-Mann Whitney test, pval< 0,0001(***).

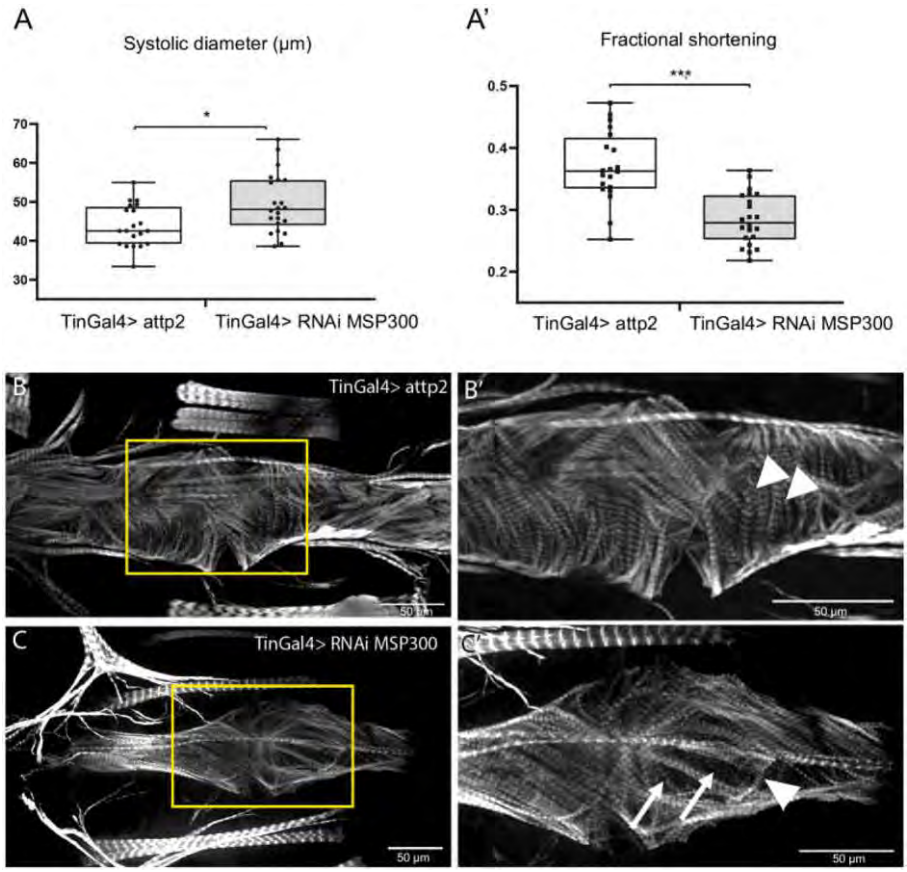

Figure 3. Cardiac-specific MSP300 KD causes reduction in contractility and myofibrillar disorganization.

(A, A') Contractility is impaired in MSP300 KD hearts from 3 weeks female flies that show an increased systolic diameter (A) and reduced fractional shortening (A') (control n=20; MSP300 RNAi n=22). Data analysis by Wilcoxon-Mann Whitney test demonstrate that the difference between controls and MSP300 RNAi is statistically significant (pval <0.0001(***)) (B) Control heart stained by F-actin show highly organized and densely packed circumferential myofibers. (B') Higher magnification view of a control heart with dense cardiomyocytes fibers (arrowheads). **(**C) MSP300 KD hearts show high disorganization of the myofibers and gaps between them. (C') Higher magnification view of MSP300 KD heart showing the lack of fibers compared to control (arrowhead) leading to gaps (arrows) between cardiomyocytes myofibers. Scale bars: 50µm

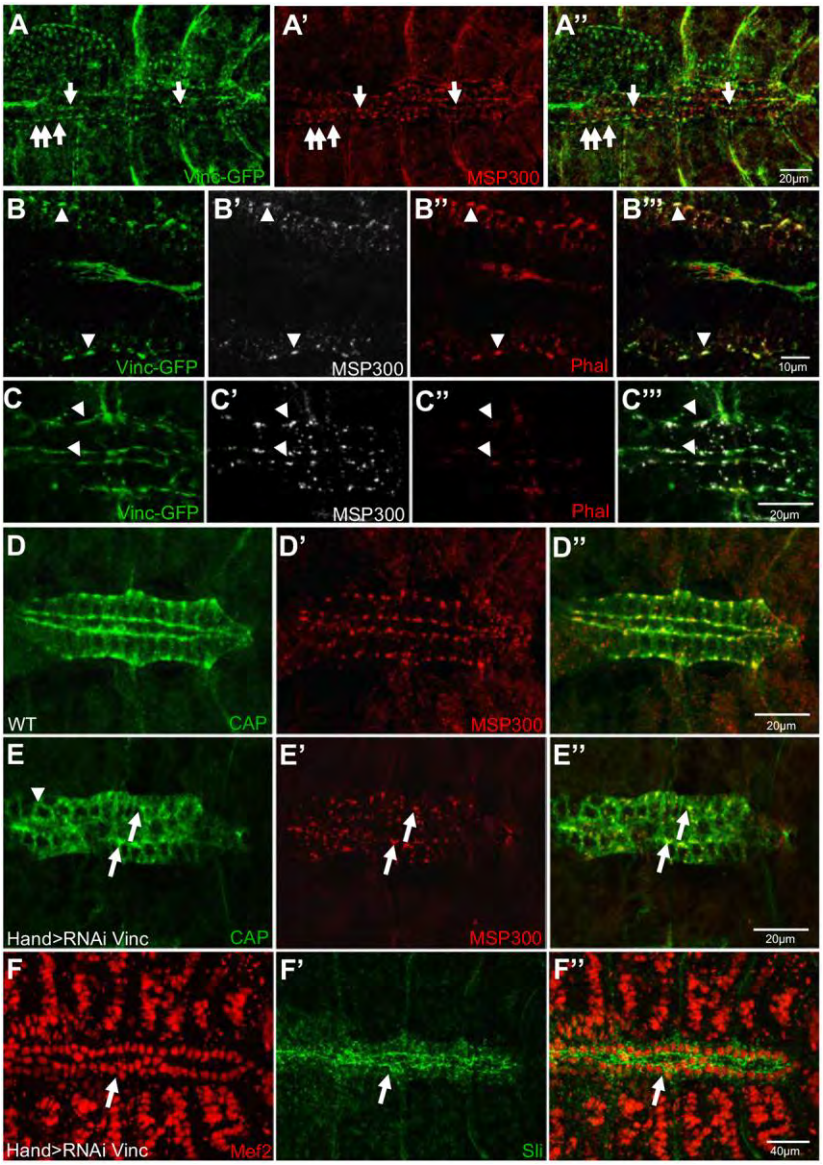

Figure 4: Vinculin controls polarized accumulation of CAP and MSP300 in CBs
(A-A") Dorsal view of stage 16 embryos revealing Vinculin-GFP localization in a spotty pattern in close proximity to MSP300 accumulation on basal and apical sides (arrows).
(B-B'") Higher magnification pictures showing that MSP300 is accumulated where the maximum of Vinc-GFP is present. Here the pictures are focused on the basal side of CBs. Vinculin partner F-actin is also present in a similar dotty pattern (B"-B'").
(C-C'") Higher magnification pictures showing that Vinculin is present at a similar level on apical side of CBs.
(D-E") Immunostainings with anti-CAP and anti-MSP300 antibodies in WT and Cardiac specific *Vinculin* KD. Accumulation of CAP and MSP300 is still visible but in a disorganized pattern (arrows) suggesting polarity defects and leading to mis-location of CBs (arrowhead in E).
(F-F") *Hand>RNAi-Vinc* leads to mis-location of CBs and affects polarized localization of Slit.

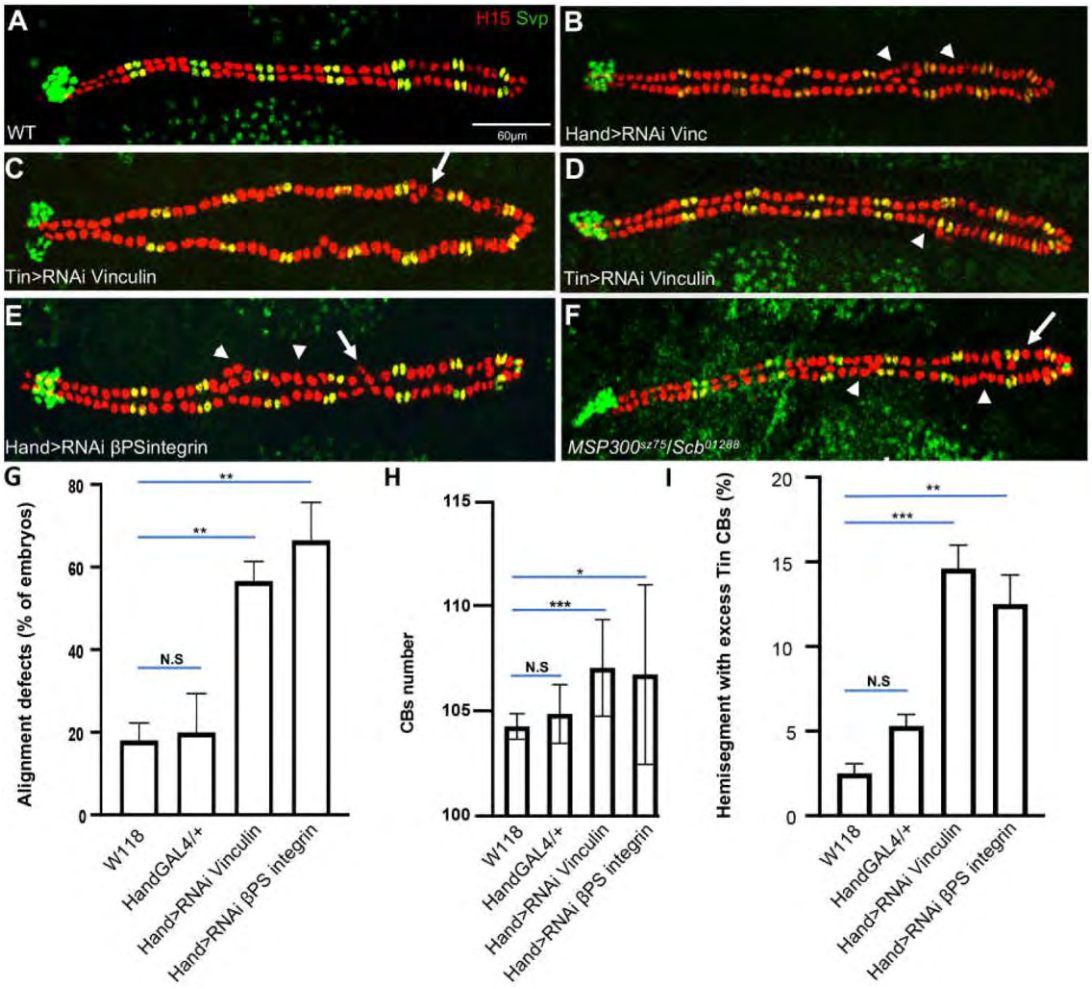

Figure 5: Vinculin/Integrin complex regulate CBs alignment and number

(A, B) Compared to WT, *Hand>RNAi-Vinc* induces a specific increase of Tin CBs in 2 hemi-segments (arrowheads)

(C-D) Cardiac cells inducible knock down of Vinculin with Tin-Gal4 driver leads to alignment defects (arrow) and increase in Tin+CBs (arrowhead) in some hemi-segments during migration leading to cardiac tube misalignment.

(E) Cardiac cells inducible knock down of βPS Integrin with Hand-GAL4 driver leads to misalignment of CBs (arrows) and an increase in Tin+CBs in some hemi-segments (arrowheads).

(F) Embryo double heterozygous mutant for *MSP300* and *alphaPS3 integrin* show similar defects of misalignment (arrows) and increase of Tin+CBs (arrowheads) suggesting a genetic interaction.

(G) Bar chart showing the percentage of embryos with CB alignment defects (n=30) Error bars represent SD; two-tailed pvalues were calculated using a Wilcoxon-Mann Whitney test, pval< 0,0001(***).

(H) Bar chart showing quantification of the mean CBs number in mentioned genetic backgrounds (n=30) Error bars represent SD; two-tailed pvalues were calculated using a Wilcoxon-Mann Whitney test, pval< 0,0001(***).

(I) Bar chart showing the percentage of hemi-segments with excess Tin+ CBs (n=240) Error bars represent SD; two-tailed pvalues were calculated using a Wilcoxon-Mann Whitney test, pval< 0,0001(***).

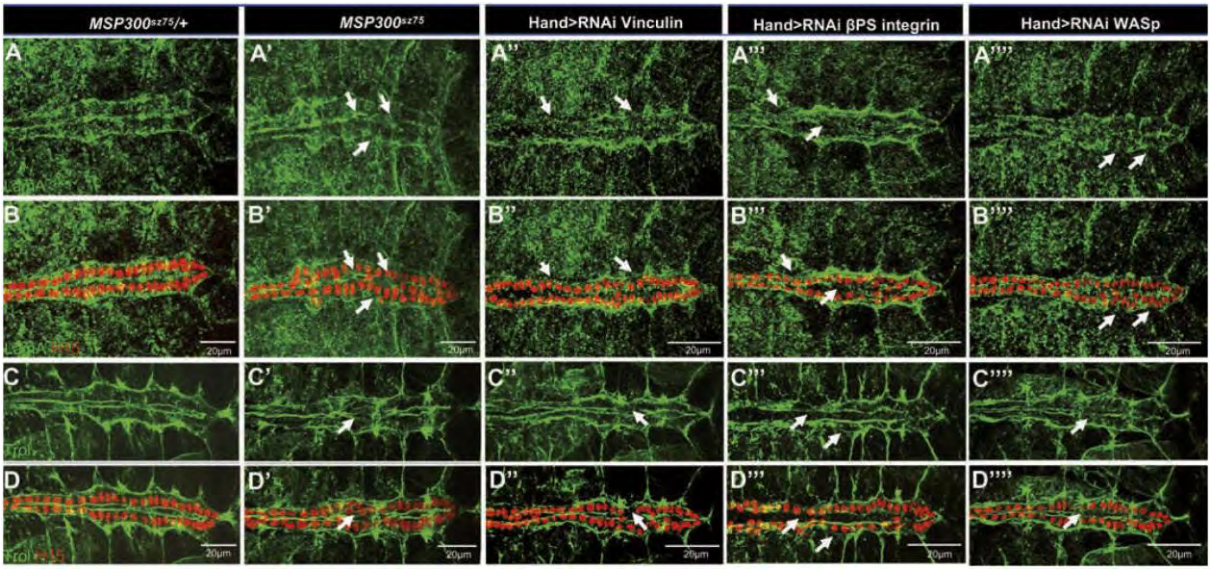

Figure 6: ECM proteins Laminin A and Trol localization is affected in MSP300, Vinculin/Integrin and WASp loss of function

(A-B') Immunostainings showing that loss of MSP300 induces a disorganized pattern of Laminin A on basal and apical sides of CBs. LamA basal layer is thinner and holes are visible around some mispositioned CBs (arrows) stained with anti-H15 antibody.

(C-D') Immunostainings showing that loss of MSP300 leads to defect in Perlecan (Trol) localization around disorganized CBs (arrow). Anti-H15 antibodies are used to stain CBs.

(A"-D") Cardiac specific KD of Vinc leads to defects in LamA and Trol localization around misaligned CBs. Arrows point discontinuous layer of ECM compared to control.

(A"'-D"') Similar results are obtained after cardiac specific KD of βPS integrin

(A""-D"") Downregulating the branched actin regulator WASp in cardiac cells leads to a disorganized pattern of ECM proteins LamA and Trol.

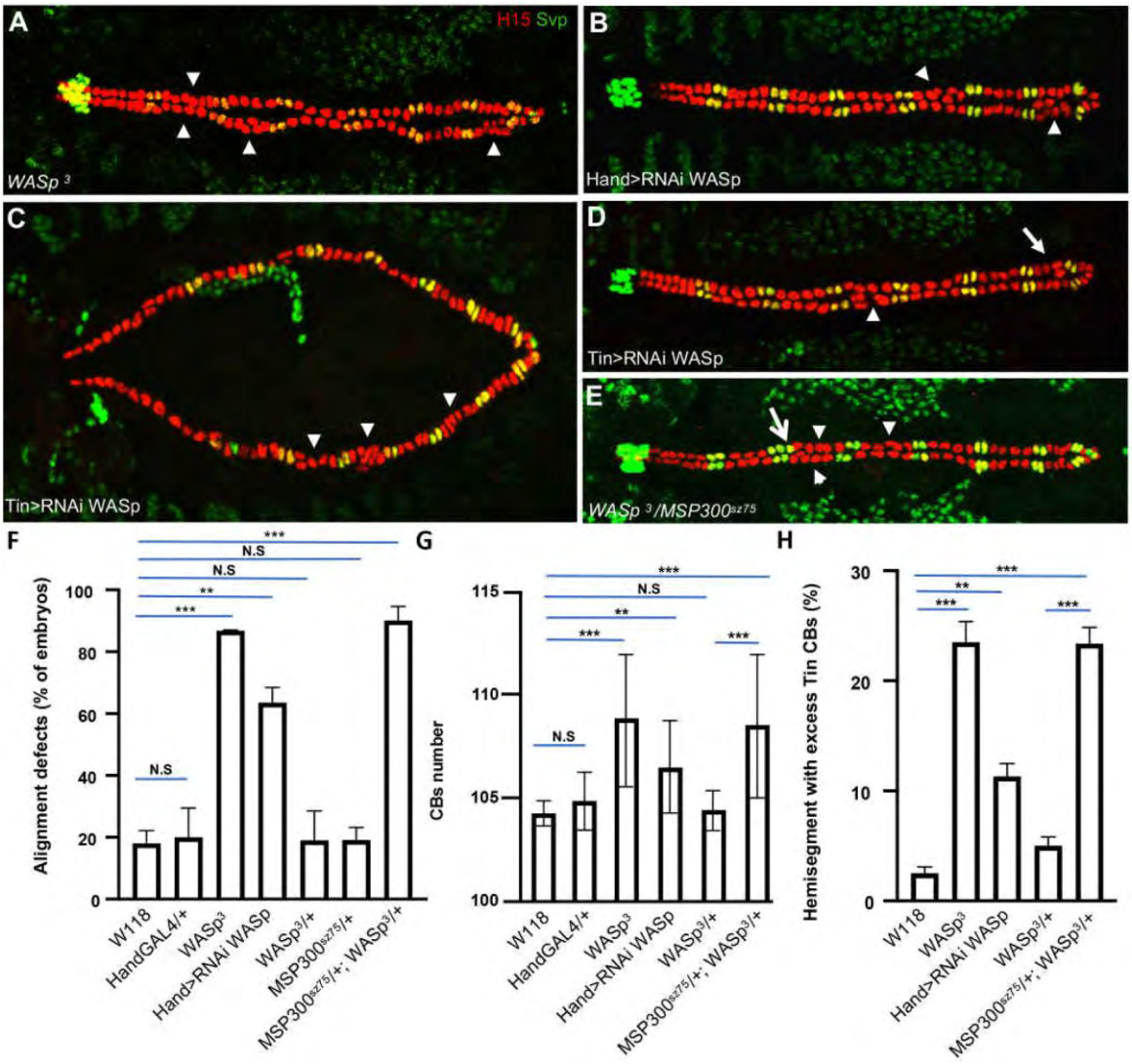

Figure 7: The Arp2/3 complex activator *WASp* interacts genetically with *MSP300* during CBs migration

(A) WASp^{3} homozygous mutant embryo showing excess of Tin+CBs in several hemi-segments (arrowheads) and closure defects.

(B) Cardiac cells inducible knock down of WASp with Hand-GAL4 driver leads to misalignment of CBs and an increase in Tin CBs in some hemi-segments (arrowheads).

(C-D) Similar defects are observed from stage 14 with Tin CBs specific driver. Arrowheads (C, D) show increased number of Tin CBs and arrow (D) misalignment without change in Tin CBs number.

(E) Transheterozygous mutant embryo for WASp^{3} and MSP300^{sz75} show increased number of Tin CBs (arrowheads) leading to alignment defects suggesting genetic interaction. Note that at lower frequency additional Svp CBs are also visible (arrow).

(F) Bar chart showing the percentage of embryos with CB alignment defects (n=40) Error bars represent SD; two-tailed pvalues were calculated using a Wilcoxon-Mann Whitney test, pval< 0,0001(***).

(G) Bar chart showing quantification of the mean CBs number in mentioned genetic backgrounds (n=30) Error bars represent SD; two-tailed pvalues were calculated using a Wilcoxon-Mann Whitney test, pval< 0,0001(***))

(H) Bar chart showing the percentage of hemi-segments with excess Tin+ CBs (n=240) Error bars represent SD; two-tailed pvalues were calculated using a Wilcoxon-Mann Whitney test, pval< 0,0001(***).

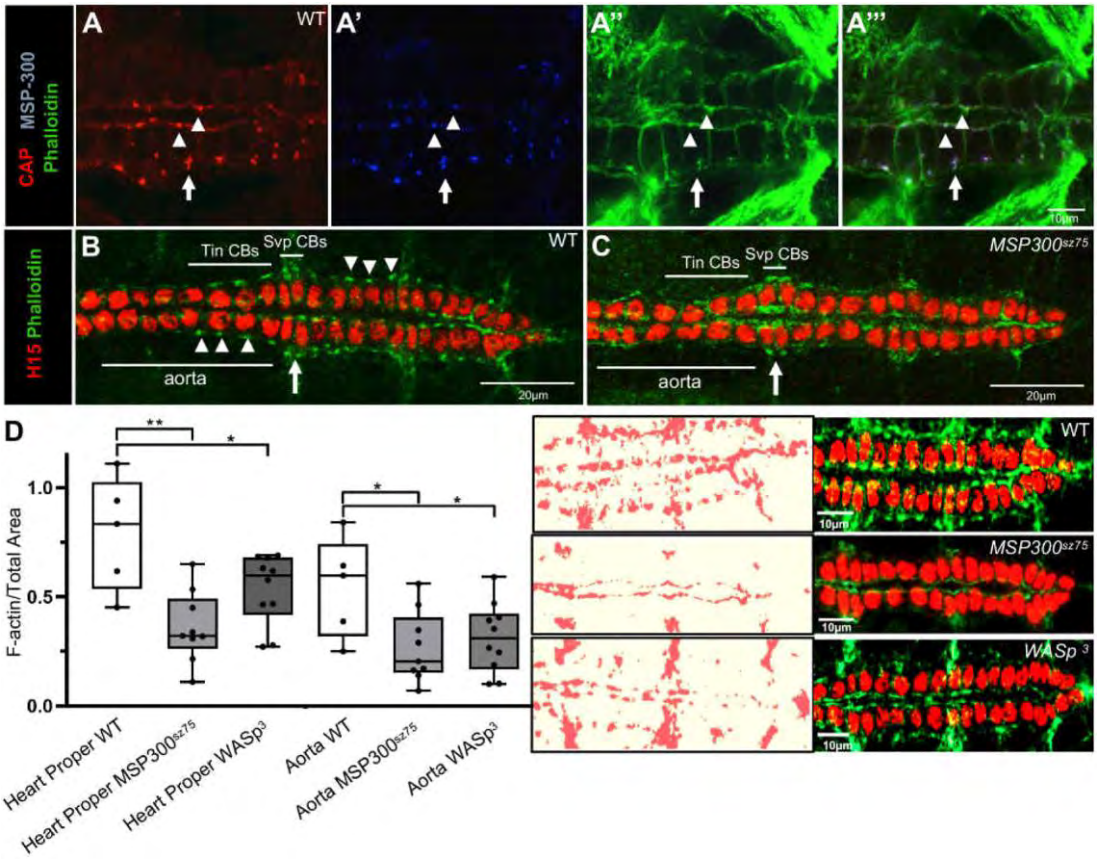

Figure 8: CAP and MSP300 mediate F-actin bridging between nucleus and integrin complex

(A-A''') Dorsal view of heart proper showing colocalization of CAP, MSP300 and F-actin on apical (arrowheads) and basal (arrows) sides of CBs showing a polarized link between nucleus and cell membrane on each side of the cells.

(B-C) Dorsal view of posterior part of the heart showing that loss of MSP300 (mildly affected embryo) leads to a decrease in F-actin polymerization more particularly in Tin CBs from aorta and heart proper (arrowheads).

(D) F-actin quantification using the Weka segmentation tool in ImageJ in heart proper and aorta

of WT, *MSP300*^{sz75} and *WASp*^{3} embryos. Unpaired two-tailed Wilcoxon-Mann Whitney test demonstrates that the difference between control and both MSP300 (heart proper pval=0,0069 (**); aorta pval= 0.0289 (*)) and *WASp* mutants (heart proper p= 0.0359 (*); aorta p= 0.0239 (*)) is statistically significant. (wild type n=5; *MSP300*-/- n= 9; *WASp* -/- n= 10). Right panels correspond to representative images of hearts stained with anti-H15 and Phalloidin from the corresponding genotypes.

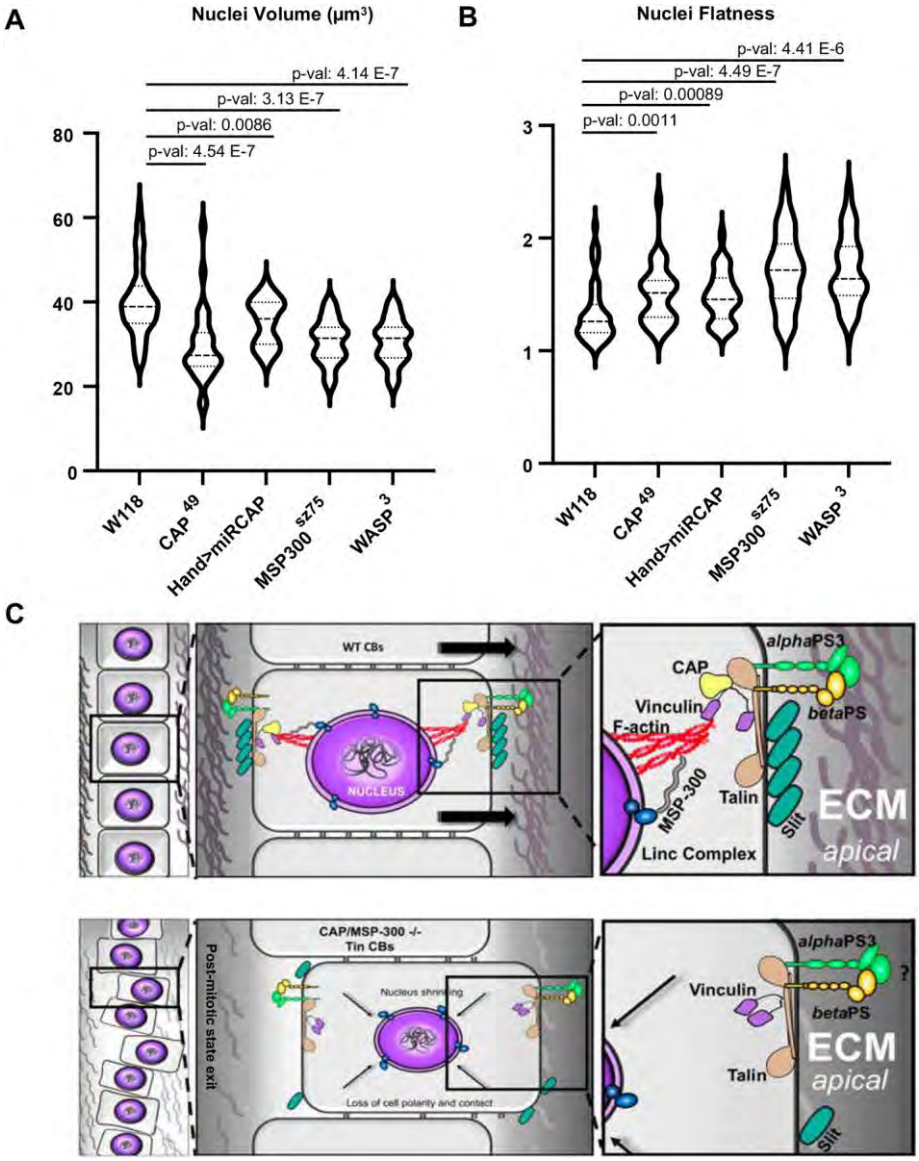

Figure 9: CAP, MSP300 and WASp maintain CBs nuclei morphology

(A-B) Nuclei morphology parameters assessment using nucleus J software in different genetic contexts. Nuclei volume is significantly reduced in *CAP*, *MSP300 and WASp* mutant CBs and in cardiac specific KD of *CAP*.

In contrary, flatness of CB nuclei increases in the same genotypes compared to W118 control.

(Two tailed p-value calculated using unpaired Wilcoxon-Mann Whitney Test, WT n=84, CAP^{49e} n=32, Hand>miRCAP n=32, $MSP300^{sz75}$ n=47, $WASp^{3}$ n=77)

(C) Model of nucleus-cytoskeleton- focal adhesion complex involving CAP adapter protein and Nesprin protein MSP300 stabilizing nuclei morphology and polarized link to cell membrane on apical and basal sides. In the loss of *CAP* or *MSP300* contexts, Vinculin interaction with F-Actin is lost, leading to a weakening of focal adhesion and affecting Slit polarization. These defects in turn induce exit from the post-mitotic state, a decrease in cell-cell contacts between neighboring CBs and misalignment within the migrating CB rows. Impact on nuclei morphology is also observed.

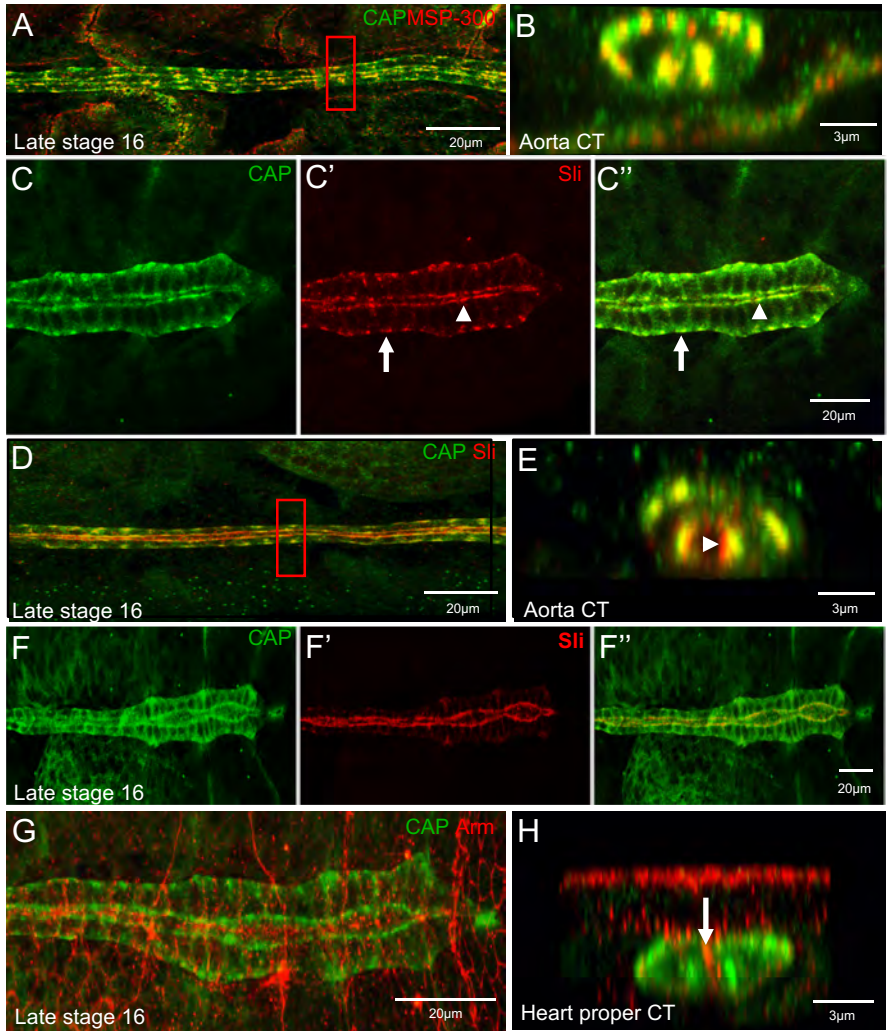

Fig. S1. CAP expression pattern in cardiac cells
(A, B) Dorsal view of a stage 16 embryo showing CAP and MSP300 localization in aorta and 3D reconstruction of transversal cut in aorta (B) validating accumulation of MSP300 and CAP on basal and apical side of CBs.
(C-C") Dorsal view of a stage 16 embryo showing that Slit colocalizes with CAP protein in a similar dotty pattern on apical (arrowheads) and basal sides of CBs (arrows).
(D, E) Dorsal view of a stage 16 embryo showing CAP and Slit localization in aorta and 3D reconstruction of transversal cut in aorta (E) validating accumulation of Slit and CAP on basal and apical side of CBs (arrowhead). Note that Slit protein is secreted at luminal side explaining the partial overlap with CAP.
(F-F") At late stage 16, Slit protein becomes accumulated at the lumen and strongly reduced at the basal side, while CAP is still maintained on both sides.
(G, H) CAP is not colocalized with Armadillo at the adherens junctions between contralateral CBs (arrow).

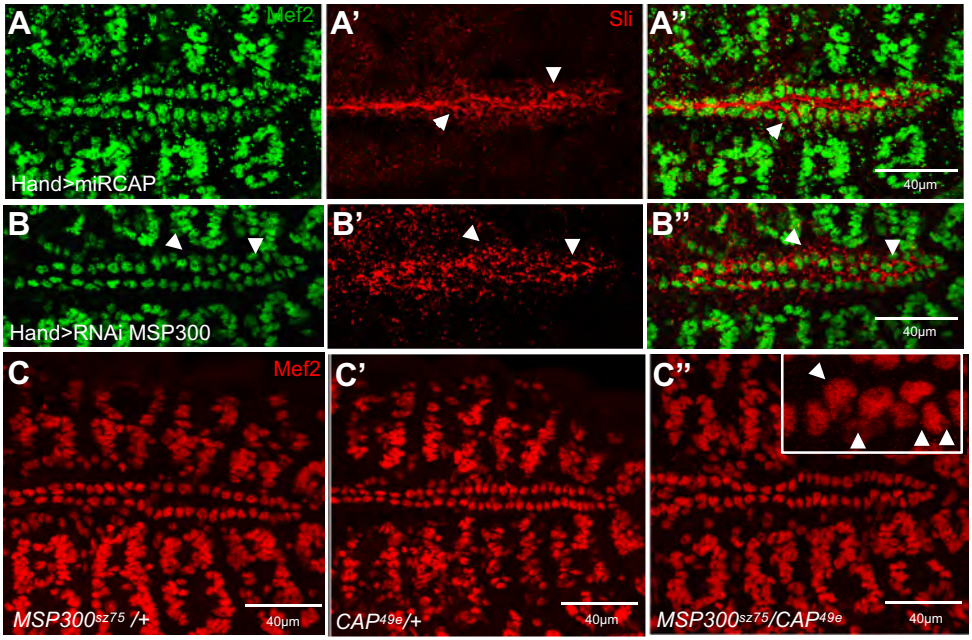

Fig. S2. CAP and MSP300 interact genetically to control CBs alignment and number (A-A") Cardiac specific miR KD of *CAP* using Hand-Gal4 driver induces CBs misalignment and polarity defects visualized with anti-Mef2 and anti-Slit antibodies (arrowheads) similarly to CAP and *MSP300* homozygous mutant. (B-B") Cardiac specific short hairpin KD (TRIP line) of MSP300 using Hand-Gal4 driver induces CBs misalignment and polarity defects visualized with anti-Mef2 and anti-Slit antibodies (arrowheads) similarly to *MSP300* homozygous mutant. (C-C") Immunostaining with anti-Mef2 in *CAP* and *MSP300* single heterozygous (C-C') by comparison with double heterozygous contexts (C"). No apparent change in CBs alignment can be observed in single heterozygous background while clusters of CBs in heart proper are visible in transheterozygous context (C", arrowheads in higher magnification window) demonstrating a genetic interaction between *CAP* and *MSP300* during CBs migration.

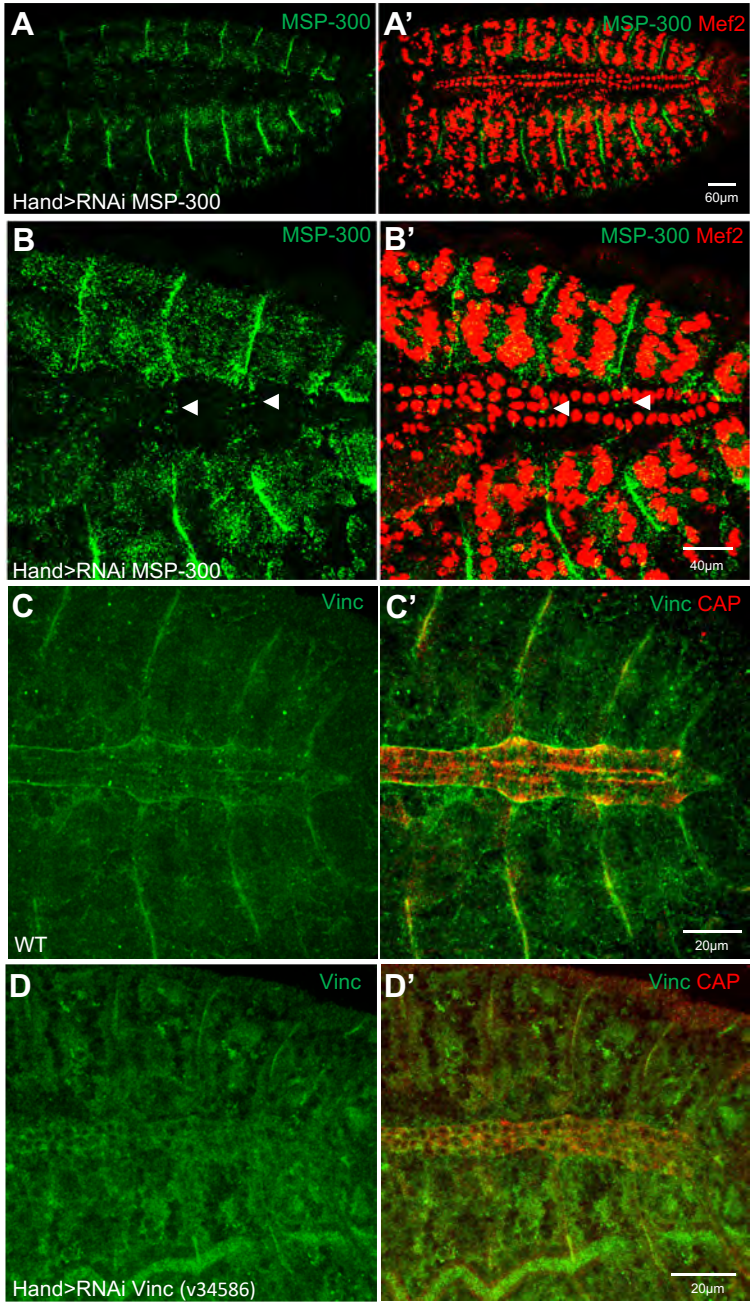

Fig. S3. Validation of RNAi lines targeting MSP300 and Vinc.
(A-B') Dorsal view of stage 16 embryo stained with anti-Mef2 and anti-MSP300 antibodies showing almost complete absence of MSP300 cardiac spots while in somatic muscles MSP300 is still highly present. Arrowheads in higher magnification pictures (B-B') point to remaining MSP300 accumulation.
(C-C') Dorsal view of stage 16 embryo stained with anti-CAP and anti-Vinc antibodies showing almost complete absence of Vinculin in RNAi context (D-D') compared to WT(C-C'). In both cases the HandGAL4 driver was used.

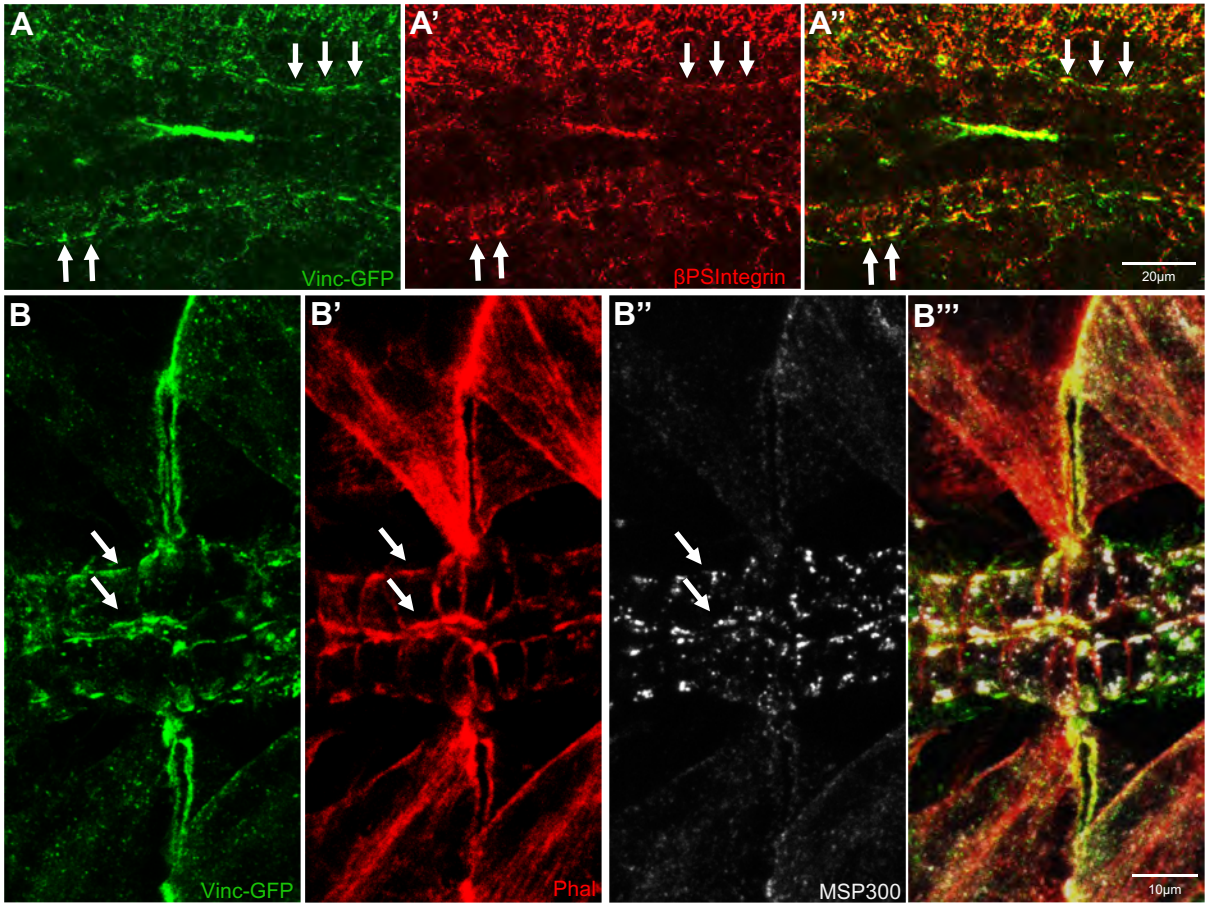

Fig. S4. Vinculin GFP colocalizes with βPS Integrin, F-actin and MSP-300
(A-A") Vinc-GFP colocalizes with bPS Integrin in cardioblasts (arrows) suggesting its involvement in Integrin focal adhesion complex. (B-B"') Dorsal view of stage 16 embryo showing Vinc-GFP colocalization with F-actin and MSP300 on apical and basal sides (arrows) suggesting a focal adhesion-based process connected to the nucleus through F-Actin.

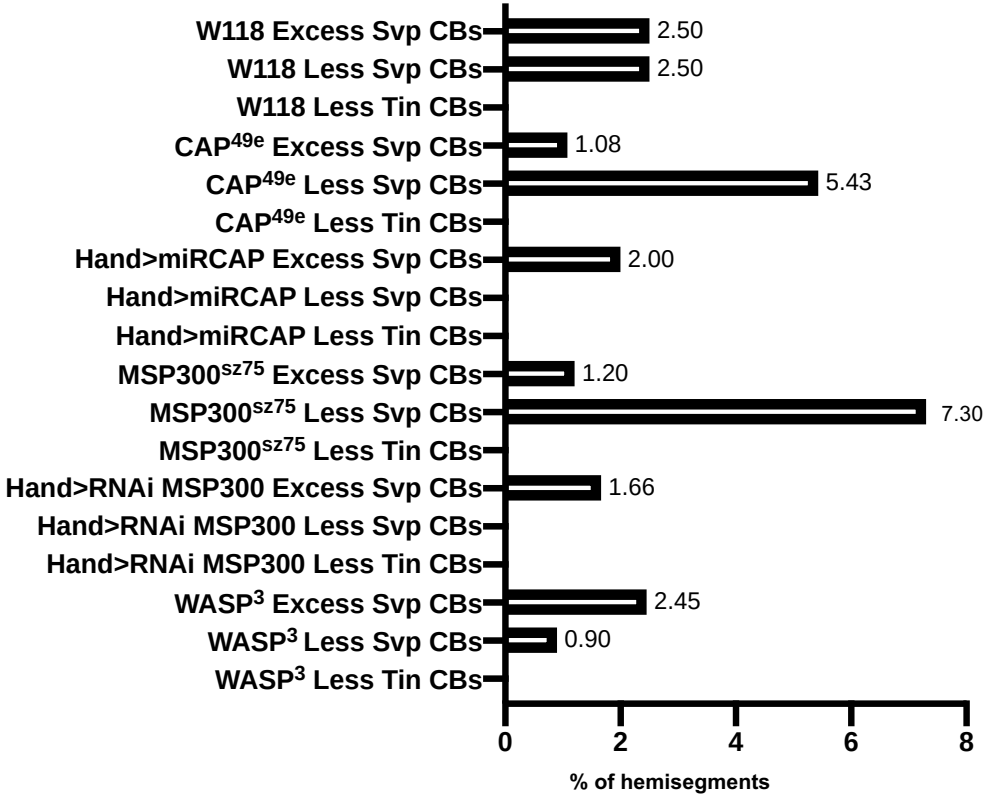

Fig. S5. Bar chart showing the percentage of hemi-segments with changes in CBs number other than an excess of Tin CBs

Data are represented as percentage of hemi-segment presenting either excess Svp +CBs, Less Svp+CBs or less Tin+CBs. (W118 n=240, *CAP49e* n=360, Hand>miRCAP n=240, *MSP300sz75* n=360, Hand>RNAi MSP300 n=240, *MSP300sz75/+* n= 240, *MSP300sz75/CAP49e* n=240, *WASp*^{3} n=240)